

# Structure-based design of inhibitors of the rice blast fungal enzyme trihydroxynaphthalene reductase

Douglas B. Jordan,\* Gregory S. Basarab,\* Der-Ing Liao,\*  
Wynona M.P. Johnson,† Kevin N. Winzenberg,† and  
David A. Winkler†

\*E. I. DuPont de Nemours and Co., Experimental Station, Wilmington, Delaware, USA

†CSIRO Molecular Science, Clayton South, Australia

*Rice Blast Disease, caused by the fungus *Pyricularia oryzae*, is one of the most important diseases of rice. Several enzymes in the melanin biosynthetic pathway have proven to be valuable targets for development of rice blast fungicides. In particular, inhibitors of trihydroxynaphthalene reductase (3HNR), which catalyzes the conversion of trihydroxynaphthalene to vermeline, have yielded commercially useful rice blast fungicides. The X-ray structure of 3HNR has been published recently, presenting an opportunity to use this information in the de novo design of novel 3HNR inhibitors that may exhibit useful rice blast activity. We used the LeapFrog program to develop a docking model for interaction of ligands with the active site of THNR. The final model gave a good correlation between calculated binding energy and log  $K_i$  and was used to design novel ligands and score compounds for synthesis. Using this as a tool, we synthesized inhibitors in the nanomolar range and also developed several inhibitors that did not conform to the properties of the THNR active site. Leapfrog was able to locate a previously unrecognized binding pocket that could accommodate these otherwise anomalous regions of structure. © 2001 by Elsevier Science Inc.*

**Keywords:** trihydroxynaphthalene reductase, de novo design, enzyme inhibitors, LeapFrog, rice blast, fungicides

Color Plates for this article are on pages 470–471.

Corresponding author: D. A. Winkler, CSIRO Molecular Science, Private Bag 10, Clayton South MDC 3169, Australia. Tel.: 61-3-9545-2477; fax: 61-3-9545-2446.

E-mail address: dave.winkler@molsci.csiro.au (D.A. Winkler)

## INTRODUCTION

Rice Blast Disease, caused by the fungus *Pyricularia oryzae*, is one of the most important diseases of rice, and causes substantial reductions in crop yields annually. Several enzymes in the melanin biosynthetic pathway have proven to be valuable targets for development of rice blast fungicides.

For the fungus to initiate disease it must undergo melanization to create a specific infection structure, the appressorium. The pathogen develops enough turgor pressure in the appressorium to punch through the leaf cells of the host plant,<sup>1,2</sup> thus penetrating the rice cuticle. Fungal melanin biosynthesis includes a pentaketide pathway that links acetate units to produce 1,3,6,8-tetrahydroxynaphthalene.<sup>3</sup> Through a series of two reductions and two dehydrations, tetrahydroxynaphthalene is transformed to 1,8-dihydroxynaphthalene, the ultimate precursor of the polymeric fungal melanin. Intermediates in this pathway include scytalone, 1,3,8-trihydroxynaphthalene, and vermeline, and the reactions are catalyzed by the enzymes scytalone dehydratase (SD) and trihydroxynaphthalene reductase (3HNR) (Figure 1).

Among the commercially-important plant diseases, rice blast stands out as the only one requiring melanin biosynthesis for infection. Consequently, enzymes of fungal melanin biosynthesis, in particular SD and 3HNR, are very suitable targets for discovering inhibitors useful for controlling blast disease in rice. Inhibitors of 3HNR, which catalyzes the conversion of trihydroxynaphthalene to vermeline, have already yielded commercially effective agents for preventing the crop disease. These include tricyclazole (1),<sup>4</sup> pyroquilon (2),<sup>5</sup> and phthalide (3)<sup>6</sup> (Figure 2). The newly commercialized carpropamid<sup>7,8</sup> is a potent inhibitor of SD (Figure 2). 3HNR and SD are particularly attractive targets for fungicide design because the biosynthetic pathway does not exist in off-target organisms and, consequently, low levels of off-target toxicity are reported for the commercial blasticides 1–3.<sup>7,8</sup>

We sought to design inhibitors of 3HNR as they have good

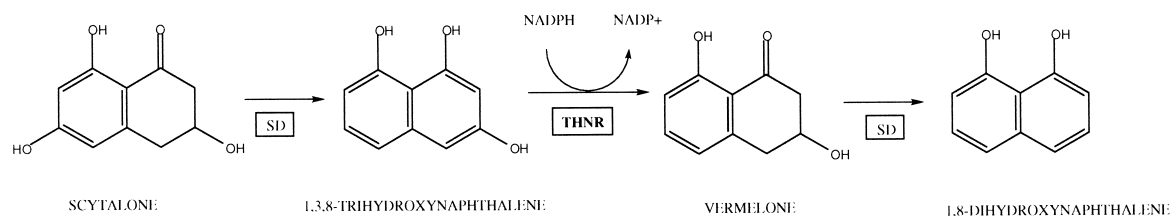


Figure 1. Relevant part of fungal melanin biosynthetic pathway: SD, scytalone dehydratase; 3HNR, trihydroxynaphthalene reductase; NADPH/NAD<sup>+</sup> reduced and oxidized form of cofactor.

potential for controlling rice blast and are likely to lack significant activity against other organisms. The X-ray structure of 3HNR in complex with tricyclazole<sup>9–13</sup> has been published recently, presenting an opportunity to use this information in the design process. There is a precedent for such an approach, as the X-ray structures of SD-inhibitor complexes<sup>9–14</sup> have been used in structure-based design of potent SD inhibitors with blasticide activity.<sup>9–13</sup> We report structure-based *de novo* design of inhibitors of 3HNR based on the X-ray structure of the native enzyme, and the enzyme with bound inhibitors.

## METHODOLOGY

### Chemistry

Structures of all standards and compounds synthesized are summarized in Table 1 and Table 2. Authentic samples of the three commercial fungicides **1–3** were obtained from commercial sources. The quinolones (**4**) and (**5**) were prepared by the procedures of Manimaran et al.<sup>15</sup> and Baron et al.,<sup>16</sup> respectively.

1,4-Benzoxazine-3-one was prepared by the procedure of Shnidhar et al.,<sup>17</sup> then alkylated with ethyl iodide under phase transfer catalysis to afford 4-ethyl 1,4-benzoxazine-3-one (**6**).

5-Trifluoromethanesulfonate-1-indanone was reacted with tributyl(vinyl)tin and Pd(PPh<sub>3</sub>)<sub>4</sub> to afford 5-vinyl-1-indanone (**7**). The analogous 5-nitro-1-indanone (**8**) was prepared by direct nitration of the precursor indanone.

Compound (**9**) was prepared by hydrogen peroxide oxidation of 5-nitroquinoline by the procedure of Coutts et al.<sup>18</sup>

The tricyclic compounds (**10**), (**11**), and (**12**) were prepared by the procedures outlined in the literature.<sup>19,20</sup>

8-Nitro-thiochromen-4-one (**13**) was prepared starting from 2-chlorothiophenol. The latter was reacted with propionic acid to give 3-(2-chlorothiophenoxy)propionic acid, followed by

sequential reaction with thionyl chloride, then polyphosphoric acid to yield compound (**13**) in good yield.

8-Nitro-1,2-dihydrobenz[d][1,3]oxazin-4-one (**14**) was prepared by the procedure of O'Sullivan et al.<sup>21</sup>

We synthesized 4*H*-imidazo[2,3-*c*]pyrido[2,3-*e*][1,4]oxazines (**15**) using the procedure of Gauthier and Duceppe.<sup>22</sup>

Compound (**16**) was prepared in a 2-step sequence by reacting aminoacetaldehyde dimethyl acetal with 2-chlorobenzoxazole, followed by treatment of the product with TiCl<sub>4</sub> in toluene.

The tricyclic compounds (**17**), (**18**), and (**19**) were made using the methods of Fusco et al.<sup>23</sup>

The imidazo[2,1-*b*]benzothiazole derivatives(**20–40**) were obtained from the condensation reaction of the appropriately substituted 2-aminobenzothiazole with freshly prepared bromoacetaldehyde.<sup>24</sup>

The 2,8-dihydroindeno[2,1-*c*]pyrazole derivatives (**41**) and (**42**) and the 4,5-dihydro-3*H*-benz[e]indazole derivatives (**43–47**) were prepared by condensation of either 1,3-dihydro-2*H*-inden-2-one or the appropriately substituted 3,4-dihydro-2(1*H*)-naphthalenone<sup>25</sup> with *N,N*-dimethylformamide dimethyl acetal followed by reaction with either hydrazine or methylhydrazine.<sup>26</sup> Compound (**44**) was obtained from palladium on charcoal mediated dehydrogenation of compound (**43**).

The imidazo[5,1-*b*]benzothiazole derivatives (**48–51**) were prepared from the appropriately substituted 2-aminothiophenol by the route reported by Avidon and Shchukina.<sup>27</sup>

The 4*H*-imidazo[1,5-*a*]benzimidazole (**52**) was made according to the general method reported by Aryuzina and Shchukina.<sup>28</sup> Compounds (**53**) and (**54**) were available commercially from Aldrich. Compound (**55**) was prepared by the procedure of Mitschker et al.,<sup>29</sup> followed by alkylation with *m*-trifluoromethylbenzyl alcohol using NaH in DMF, followed by column chromatography on silica gel.

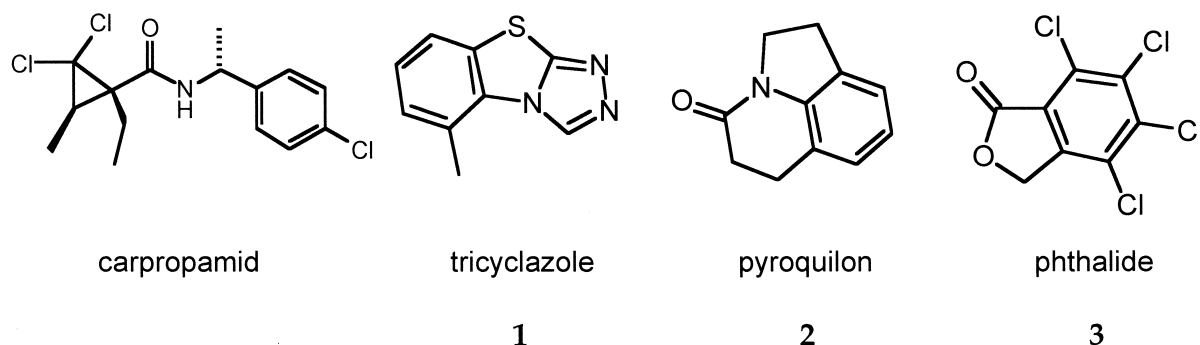
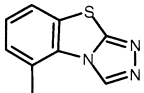
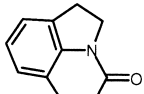
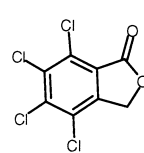
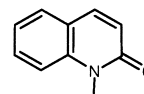
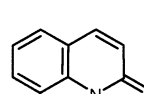
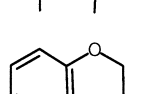
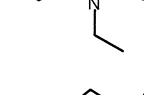
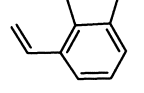
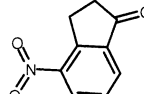
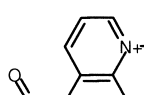
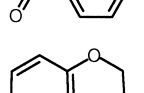
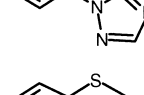


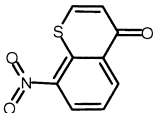
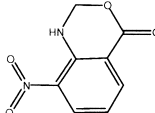
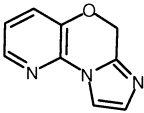
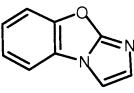
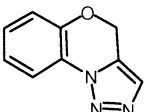
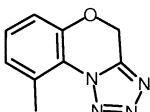
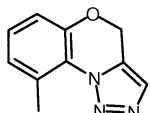
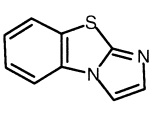
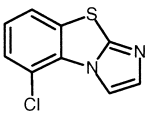
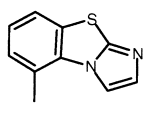
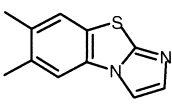
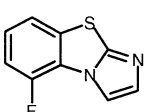
Figure 2. Commercial blasticides that target melanin biosynthesis. Capropamid inhibits SD, and the others inhibit 3HNR.

**Table 1. Measured and predicted 3HNR activities and Leap Frog binding energies of typical binders**

	Compound	Ki (nM)	pKi	Log P	LeapFrog Binding energy (kcal/mol)	Predicted pKi
1		2	8.70	2.950	−38.357	8.33
2		2	8.70	2.230	−36.595	7.87
3		2	8.70	4.060	−36.372	7.82
4		120	6.92	1.810	−34.950	7.45
5		48	7.32	2.350	−35.910	7.70
6		460	6.34	2.210	−30.150	6.21
7		390	6.41	2.460	−31.750	6.63
8		38	7.42	1.610	−35.563	7.61
9		640	6.19	1.680	−30.400	6.28
10		2200	5.66	2.50	−29.720	6.10
11		2900	5.54	2.710	−27.629	5.56
12		250	6.60	3.16	−31.294	6.51

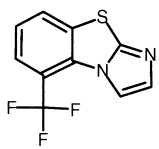
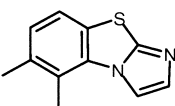
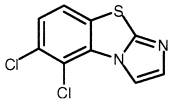
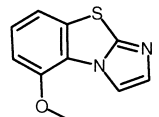
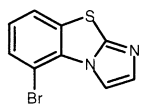
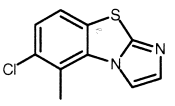
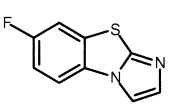
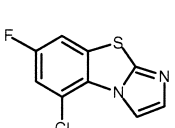
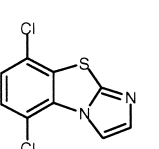
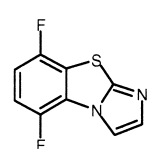
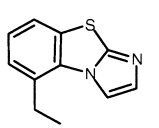
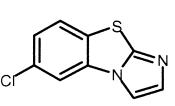
(Continued)

**Table 1. (Continued)**

	Compound	Ki (nM)	pKi	Log P	LeapFrog Binding energy (kcal/mol)	Predicted pKi
13		20	7.70	1.680	−35.094	7.49
14		200	6.70	1.230	−34.862	7.43
15		9600	5.02	1.600	−27.043	5.41
16		6500	5.19	1.070	−26.104	5.171
17		470	6.33	1.390	−31.527	6.57
18		20	7.70	2.10	−35.858	7.68
19		45	7.35	2.050	−33.319	7.03
20		670	6.17	2.040	−29.289	5.99
21		3.4	8.47	2.750	−37.540	8.12
22		28	7.55	2.700	−33.228	7.01
23		6300	5.20	3.240	−27.000	5.40
24		23	7.64	2.180	−33.800	7.15

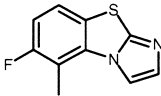
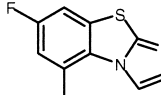
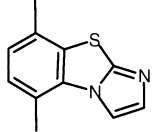
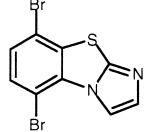
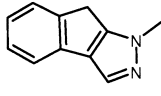
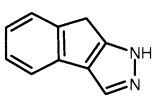
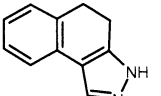
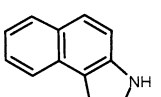
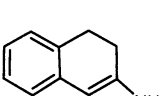
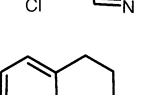
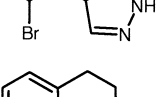
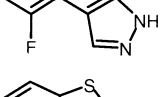
(Continued)

Table 1. (Continued)

	Compound	Ki (nM)	pKi	Log P	LeapFrog Binding energy (kcal/mol)	Predicted pKi
25		70	7.15	2.560	-35.736	7.65
26		610	6.21	3.240	-34.913	7.44
27		13	7.89	3.340	-34.940	7.45
28		2100	5.68	2.340	-29.555	6.06
29		4.6	8.34	2.900	-36.800	7.93
30		58	7.24	3.290	-34.579	7.35
31		5400	5.27	2.120	-29.749	6.11
32		110	6.96	2.710	-30.926	6.41
33		5	8.30	3.340	-33.600	7.10
34		16	7.80	2.140	-32.518	6.82
35		580	6.24	3.240	-30.176	6.22
36		870	6.06	2.750	-32.283	6.76

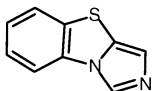
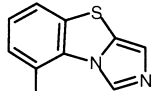
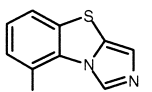
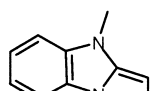
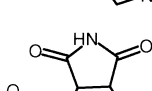
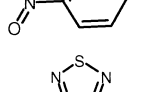
(Continued)

Table 1. (Continued)

	Compound	Ki (nM)	pKi	Log P	LeapFrog Binding energy (kcal/mol)	Predicted pKi
37		19	7.72	2.660	-37.000	7.98
38		770	6.11	2.660	-31.806	6.64
39		46	7.34	3.240	-30.800	6.38
40		7.9	8.10	3.64	-28.36	5.75
41		17000	4.77	1.87	-23.723	4.56
42		810	6.09	1.000	-29.642	6.09
43		87	7.06	1.58	-34.573	7.35
44		130	6.89	1.94	-31.624	6.60
45		5.6	8.25	2.290	-38.800	8.44
46		7.9	8.10	2.440	-40.200	8.80
47		12	7.92	1.72	-31.860	6.65
48		1600	5.80	3.300	-34.231	7.26

(Continued)

Table 1. (Continued)

	Compound	K <sub>i</sub> (nM)	pK <sub>i</sub>	Log P	LeapFrog Binding energy (kcal/mol)	Predicted pK <sub>i</sub>
49		130	6.89	2.640	−31.700	6.61
50		20	7.70	3.300	−34.720	7.39
51		43	7.37	3.350	−33.837	7.16
52		380	6.42	3.270	−32.780	6.89
53		920	6.04	.180	−31.320	6.51
54		220	6.66	.730	−26.900	5.38

The 2-trichloromethylquinazolin-4(3*H*)-one derivatives (**56–66**) were prepared by displacement of the 4-chloro substituent of 2-trichloromethyl-4-chloroquinazoline with the sodium salts of the respective alcohols or hydroxylamine in DMF, followed by chromatographic purifications. The corresponding 2-chloroquinazolin-4(3*H*)-one derivatives (**67–69**) were prepared similarly from 2,4-dichloroquinazoline. 2,4-Dichloroquinazoline was prepared by methods described elsewhere.<sup>30,31</sup>

The thienopyrimidine derivative (**70**) was prepared similarly to the above starting from 3*H*-thieno[2,3-*d*]pyrimidin-4-one.<sup>32</sup>

The structures were confirmed by <sup>1</sup>H NMR and by mass spectroscopy.

### X-ray Crystallography and Active Site Topography

The X-ray diffraction data were collected at −168°C on a Raxis-IV imaging plate system. Co-crystallization of 3HNR with **1** and **2** and NADPH, data collection, and refinement were conducted by the methods of Andersson et al.<sup>33</sup> with some modifications. The structure, solved at 2.1 Å resolution, provided an excellent model according to the refinement statistics and by visual inspection of the electron density surrounding the inhibitor, NADPH, and the protein. We also solved the structure with various inhibitors, such as tricyclazole (**1**), pyroquilon (**2**), and compound **8**, bound to the active site.<sup>34,35</sup> Molecular replacement and initial refinements were performed with both NADPH and the inhibitor removed.

### Determination of Inhibition Constants

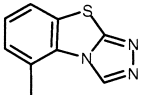
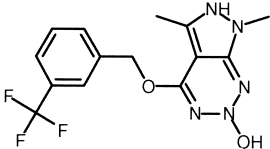
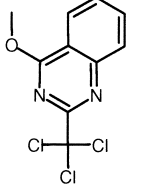
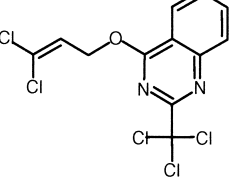
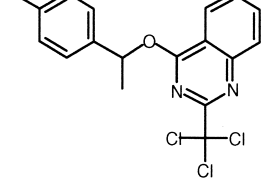
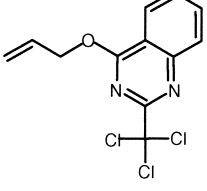
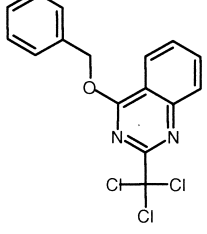
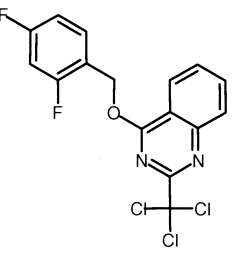
The assay for determining inhibition constants was biased for the formation of 3HNR-NADPH-inhibitor complexes because tricyclazole is known to bind considerably tighter in this complex than in the ternary complex with 3HNR-NADP<sup>+</sup> or in the binary complex with 3HNR.

Assay mixtures (1 mL) included 100 mM MOPS-NaOH, 0.1 mM NADPH, 9 nM 3HNR (active sites), and 20 μM phenanthrene quinone (PQ), at pH 7.0 and 25°C (1). DMSO (5 μL), in the absence or presence of inhibitor, was added 10 s before initiating reactions with PQ in 5 μL DMSO. Initial rates were determined by monitoring NADPH consumption continuously at 340 nm using a HP 8542A spectrophotometer (Hewlett Packard) for 60 s. IC<sub>50</sub> values were determined by fitting the initial rate data to equation 1:  $\nu$  is the observed velocity;  $V_o$  is the uninhibited observed velocity;  $I$  is the inhibitor concentration; and IC<sub>50</sub> is the concentration of inhibitor affording 50% inhibition. Competitive inhibition was

$$\nu = \frac{V_o}{1 + I/IC_{50}} \quad (1)$$

determined for the more potent (IC<sub>50</sub> < 1 μM) inhibitors described. In addition to the compounds described, other structurally similar inhibitors have been found to bind in the substrate pocket from X-ray crystallographic studies (2,3). Therefore, K<sub>i</sub> values were calculated from the IC<sub>50</sub> values by using the relationship of Equation 2. A is the substrate con-

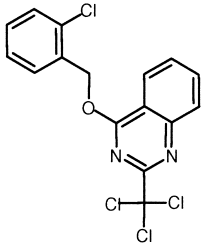
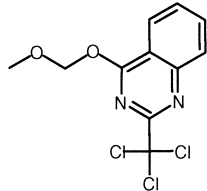
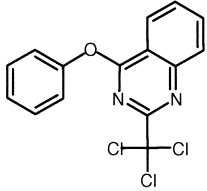
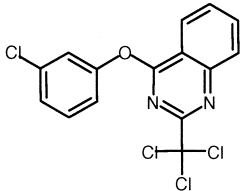
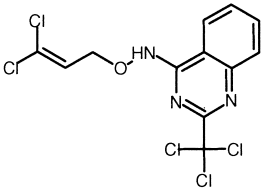
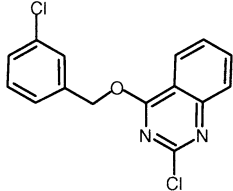
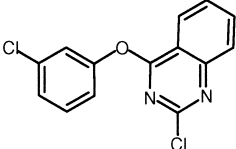
**Table 2. Measured 3HNR activities and logP values of atypical binders**

	Compound	Ki (nM)	pKi	Log P
1		2	8.70	2.95
55		440	6.36	6.67
56		290	6.54	3.19
57		35	7.46	3.01
58		4800	5.32	5.80
59		170	6.77	3.72
60		1800	5.74	4.74
61		2400	5.62	4.65

*(Continued)*

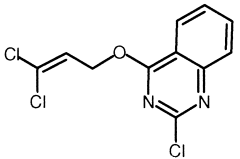
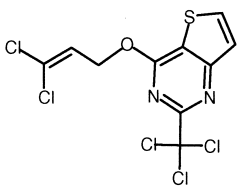


Table 2. (Continued)

	Compound	Ki (nM)	pKi	Log P
62		2200	5.66	5.33
63		2400	5.62	2.73
64		4900	5.31	5.10
65		630	6.20	5.69
66		1800	5.74	2.53
67		1700	5.77	4.66
68		6400	5.19	5.02

(Continued)

Table 2. (Continued)

	Compound	K <sub>i</sub> (nM)	pK <sub>i</sub>	Log P
69		1700	5.77	2.34
70		1100	5.96	2.55

centration;  $K$  is the Michaelis constant ( $K = 5.0 \mu\text{M}$  from several determinations); and  $K_i$  is the dissociation constant for the inhibitor from the ternary 3HNR-NADPH-inhibitor complex. In practice, the  $\text{IC}_{50}$  values were divided by 5 to generate  $K_i$  values.

$$K_i = \frac{\text{IC}_{50}}{1 + A/K} \quad (2)$$

3HNR assays were carried out on all candidates using a published procedure.<sup>36</sup> Results are summarized in Tables 1 and Table 2 with  $K_i$  values in nanomolar.

## Molecular Modelling

The X-ray structures of 3HNR with and without bound ligands were checked for consistency and correct atom types, and hydrogens were added. Atom charges were assigned using the Kollman all-atoms dictionary method.<sup>37,38</sup> Molecular structures were constructed using Sybyl 6.5 and optimized using the Tripos force field<sup>39</sup> with default parameters. The docking experiments were performed using the LeapFrog method. This allows a stochastic optimization of ligands into the active site and is a flexible modelling method allowing considerable control over the types of interactions contributing to the calculated binding energy. It will also attempt to optimize ligand structure by structural modification, e.g., by exchange of functional groups, conversion of aromatics to heteroaromatics, ring fusion, and addition of new functionality.

In LeapFrog, binding energy is calculated from three major components: the direct steric, electrostatic, and implicit hydrogen bonding enthalpies of ligand-cavity binding, calculated using the Tripos force field.<sup>39</sup> The program also allows use of an optional cavity desolvation energy, an optional incremental hydrogen bonding energy, and an optional ligand desolvation energy, estimated from a very simple model.

In general, the method of calculating binding energies in LeapFrog is similar to that of Goodford's GRID program.<sup>40</sup> However, in LeapFrog, ligand atom coordinates are binned to increase speed and the binding energy of each ligand atom is calculated as though the atom were actually located in the center of a cube containing that atom. A simple linear expression then yields the energy of interaction between the site and

that particular ligand atom. Summing over all ligand atoms yields the overall site-ligand interaction energy.

We did not use explicit hydrogen bond terms, as the implementation in LeapFrog was too inflexible. The electrostatic approximation used for implicit hydrogen bonds appeared to work well for 3HNR ligands where hydrogen bonding between the ligand acceptor atoms(s) and the active site donor residues Ser164, Tyr178 was important. We used Gasteiger-Huckel charges on the ligand atoms and dictionary charges on the enzyme. In the case of ligands containing imidazoles we found that Gasteiger-Huckel charges did not correlate with the stronger hydrogen bond acceptor strength of these rings<sup>41</sup> and we used MMFF charges in these cases.

In most cases LeapFrog was used to optimize the position of ligands within the active site and to minimize the binding energy. This was done using optimize mode in LeapFrog with an average of 20,000 TWIST and FLY moves (in 3:1 ratio). TWIST moves allow conformational relaxation of flexible bonds within the ligand and FLY moves allow rigid body rotations and translations within the site. FLY moves were chosen stochastically up to 3 Å translation and 60° rotation. Site points were calculated for lipophilic and charged atoms in the site. The site point box was chosen large enough to encompass all residues in the active site. We did not use the optional cavity desolvation terms and ran computational experiments with and without the optional ligand desolvation terms. We found the best correlation with log  $K_i$  values using the binding energies ignoring the optional ligand desolvation terms. Binding energy minimization was carried out before evaluating the fitness of any moves, and strain minimization was done after TWIST moves. Default values were used for the other LeapFrog settings.

LeapFrog was also used in an additional optimization mode for designing improved inhibitors. In this case a core structure was defined and positions of possible substitution defined. LeapFrog stochastically selected functional groups for substitution from a library and attached them to the substitution positions and the resulting new inhibitor was optimized in the site as previous inhibitors had been. The fragment library used was adapted from the Sybyl fragment library used for building structures, not the much more limited default fragment library provided with LeapFrog.

Docking calculations were carried out using the implemen-

tation in Sybyl 6.5, which uses the Tripos force field. Both the ligand and enzyme structures were considered flexible during the docking calculation of the atypical inhibitors in the site.

## Active Site Properties

The active site is essentially disk-shaped (see Color Plate 1), with the hydrogen bond donors Ser164 and Tyr 178 on one edge (Color Plate 2). The majority of the site is lipophilic. The crystal structure shows that all inhibitors are sandwiched between the nicotinamide ring of NADPH and the phenol ring of Tyr223. Hydrogen bond acceptor groups, such as carbonyl oxygen atoms or heterocyclic nitrogen atoms, are oriented toward the hydrogen bond donor OH groups of Ser164 and Tyr178. Color Plate 2 and Figure 3 show hydrogen bond interactions between these residues and inhibitor **8**. Other ring substituents, such as the nitro group in **8**, are oriented toward a lipophilic region occupied by Tyr216 and Cys220. Distances of key interactions are listed in Figure 3. When all the active site orientations of inhibitor structures are superimposed on that of 3HNR complexed with tricyclazole and NADPH,<sup>33</sup> the inhibitors occupy nearly the same space (Color Plates 3 and 5). The hydrogen bond acceptor groups lie in a small region of space near the two donor residues Ser 164 and Tyr 178 with the carbonyl oxygen of **8** bisecting the adjacent nitrogen atoms of tricyclazole. There is negligible movement of active site sidechain residues involved in inhibitor interactions between the crystal structures of 3HNR bound to different inhibitors. Consequently the shape of the site is relatively conserved, lending confidence to its use in the design of new inhibitors.

## Inhibitor Design

The site shape, lipophilicity, and hydrogen bond donor properties were used to design novel ligands. These ligands were generally lipophilic and flat, with strong hydrogen bond acceptor groups on one edge like the commercial inhibitors. The site dimensions provided a limit to the size of the planar ring structures chosen. As hydrogen bond acceptors on the inhibi-

tors were crucial for activity, we used the work of Abraham et al.<sup>41</sup> to chose the most appropriate functional groups to append to the planar, lipophilic cores. For example, imidazoles are substantially better hydrogen bond acceptors than pyrazoles or triazoles.<sup>41</sup> We also attempted to exploit the greater hydrogen bond affinity of vinylogous amides and esters in inhibitors.<sup>42</sup>

Using the above criteria we developed the inhibitors shown in Table 1. These compounds showed reasonable structural diversity and exhibited a range of  $K_i$  values in 3HNR. A larger number of compounds were screened, but only compounds exhibiting  $K_i$  values below 20  $\mu$ M (20,000nM) are reported here. There was considerable ambiguity in how these poorly active compounds interacted with 3HNR, as many were conformationally flexible and some poorly active agents can work as allosteric inhibitors. Choosing a cutoff of 20  $\mu$ M gave us a range of  $K_i$  values spanning 4 orders of magnitude.

Log P (octanol/water) values were calculated using the HINT! package.<sup>43</sup> The optimum log P value for systemic effectiveness in rice plants was known to be approximately 2.5 (the values of the commercial standards).

## RESULTS AND DISCUSSION

### Conventional Inhibitors

Using the parameters for LeapFrog reported above, we calculated an energy of interaction between the inhibitors and the 3HNR active site. These energies are summarized in Table 1. We found a good correlation between the calculated binding energy of the ligands and the log  $K_i$  values measured in the assay. The correlation shown in Color Plate 4 was:

$$-\log K_i = pK_i = -1.55(\pm 0.782) - 0.258(\pm 0.024) \text{ BE (kcal/mole)}$$

$$n = 52, r^2 = 0.703, \text{ SEE} = 0.575, F = 118.1,$$

$$p > 99.99\% \quad (3)$$

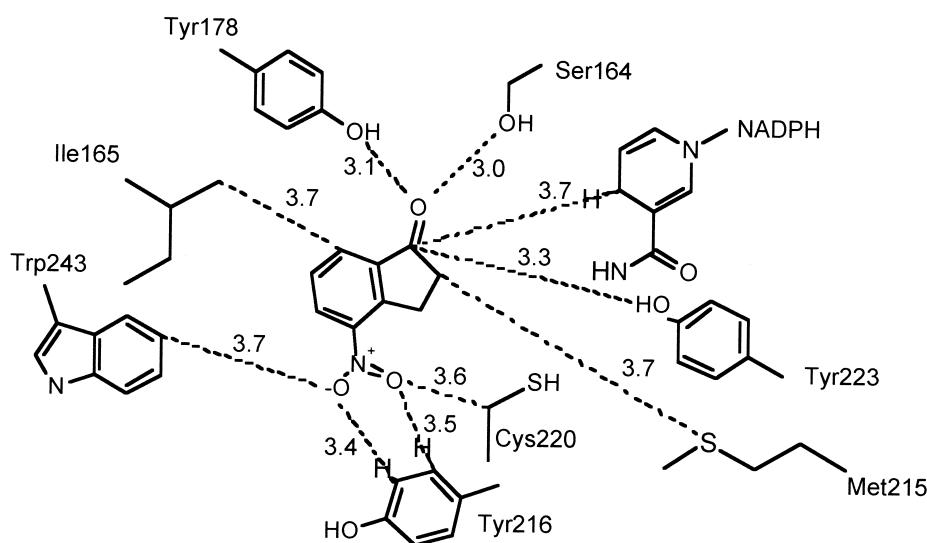


Figure 3. Binding of 5-nitro-1-indanone **8** within the active site of 3HNR showing interactions with key residues. Distances are in Å.

where  $n$  is the number of compounds,  $r$  is the correlation coefficient, SEE is the standard error of estimation,  $F$  is the F-statistic, and  $p$  is the significance of the regression. This consistent relationship between the empirical binding energy and measured  $pK_i$  and the conserved active site geometry with different inhibitors gave us confidence in the ability of LeapFrog to predict activities of new analogs. We used LeapFrog to suggest designs for putative inhibitors and rank synthesis candidates before carrying out the chemistry. Some compounds were poorly modelled using these techniques. The binding energies of compounds **40** and **54** were consistently underestimated. Compound **40** contains para bromo substituents and its low calculated binding energy may reflect a deficiency in the force field for this type of compound. Compound **54** is a benzothiadiazole and its poor binding energy may reflect either underestimated hydrogen bond acceptor affinity of its heterocyclic nitrogen atoms, or an overestimate of the influence of heterocyclic sulfur atoms. The optimum location of the inhibitors in the active site was consistent with the binding of the commercial compounds **1–4**, with the lipophilic rings sandwiched between the nicotinamide ring of NADPH and the phenol ring of Tyr223, and the hydrogen bond acceptor groups lying approximately 2.7 Å from the active site donor atoms of Ser164 and Tyr 178.

Apart from the relatively good correlation between the calculated binding energies and the  $pK_i$  values, we validated the results of the LeapFrog optimizations by perturbing the positions of the commercial fungicides **1–3** within the active site and allowing LeapFrog to optimize them. We found that the optimized positions agreed very well with the positions from the crystallographic studies. In the case of pyroquilon, which theoretically could bind in two orientations (one with the structure flipped 180°), we used LeapFrog to predict the correct binding orientation before the crystallographic position being determined. The crystallographic location was consistent with the predictions.

Color Plate 5 shows the predicted binding mode of three of the more active imidazole inhibitors (**21**, **29**, and **33**) developed in this study. In each case one of the imidazole atoms acts as the hydrogen bond acceptor while the lipophilic halogen substituents occupy a lipophilic pocket formed by Tyr216, Cys220 and Met215.

### Atypical Inhibitors

We also discovered a class of nonplanar inhibitors on the basis of some accessible chemistry. These structures had the planar lipophilic rings and hydrogen bond acceptor moieties found in the other inhibitors, but they also had another generally lipophilic group joined to the main structure by a relatively flexible linker. The low energy conformations of this class of compound had the additional moiety extending out of the ring plane. These compounds are summarized in Table 2. They could not be accommodated in the active site region in which the others bound, as the additional substituents were nonplanar and did not fit this site, creating unfavorable steric contacts. Initially the binding of these was explained by the observation that the 3HNR active site is capped by a flexible “lid” that opens to admit substrates or inhibitors.<sup>44</sup> We hypothesized that these atypical inhibitors were able to enter the site when the lid (consisting of residues 214–244 and forming a helix-loop-helix region) was open, and the lid closed down only partially to

accommodate the out-of-plane portion of the inhibitor structure. However, during a LeapFrog optimization run when new substituents were being added stochastically to an existing inhibitor structure, LeapFrog located a hitherto unrecognized binding mode that could accommodate these novel, nonplanar inhibitors. The nonplanar part of the inhibitors appears to bind into a narrow cleft bounded by Gly210, Cys220, Trp243, and Met283. The aryl group, or equivalent, of the atypical inhibitors, which occupies this pocket, lies parallel to the ring of Trp243. Given that this pocket encompasses the lid region of 3HNR, it provides a mechanism for how the lid folding down can accommodate atypical inhibitors.

Sybyl Dock calculations were used to derive a likely structure for 3HNR with atypical inhibitors bound. The 3HNR structure changed slightly in the active site region. Color Plate 3 shows the difference between the position of important residues in the X-ray structure containing tricyclazole **1**, compared with that from the Dock calculations. Dock calculations allowing the ligand and receptor to flex show this pocket opening up slightly (i.e., Trp243 and Gly210 move slightly apart from each other; see Color Plate 6), with considerable reduction in steric energy. Due to the conformational flexibility of the atypical ligands, and the need to optimize the inhibitor–enzyme complex for each inhibitor, we did not attempt to calculate relative binding energies for these compounds.

Color Plate 7 shows atypical inhibitors superimposed, showing that they all occupy the site in similar orientations. Color Plate 8 shows the structure of **57** in the orientation predicted by LeapFrog in the 3HNR site. Also shown superimposed are the structures of tricyclazole **1** and pyroquilon **2**, illustrating where the new, nonplanar pocket lies with respect to the tricyclazole binding pocket. Attempts to obtain X-ray structures of 3HNR with an atypical inhibitor bound to the active site to verify this predicted binding mode were unsuccessful.

### CONCLUSIONS

Clearly the properties of the 3HNR active site, and the LeapFrog method, were very useful in designing new inhibitors of this enzyme.

Existing inhibitors, and those designed by our *de novo* approach, appear to fill the circular, flat site nearly optimally. It is difficult to devise any new ring systems or hydrogen bond acceptors that can bind more strongly than pyroquilon or tricyclazole. Several of our most active enzyme inhibitors showed significant rice blast activity *in vivo*, provided that their log P values were similar (~2.5) to those of the commercial agents **1** and **2**. However, the discovery of a novel out-of-plane binding pocket occupied by the atypical inhibitors provides scope to design new inhibitors with  $K_i$  values below 1nM. Any new inhibitors would need to have a planar bicyclic or tricyclic structure with suitable hydrogen bond acceptors that could also carry a substituent (e.g., a flat, 6-membered ring) able to access the new pocket through a flexible linkage. This would require an  $sp^3$ -hybridized carbon atom in the base structure, probably one that is part of a constrained 5-membered ring (to reduce flexibility). These new inhibitors should be able to gain all of the binding energy of Tricyclazole and related inhibitors plus additional binding from the extra pocket. These leads should be more novel and further from the current patent art than purely planar leads.



## REFERENCES

- Howard, R.J., and Ferrari, M. A. Role of Melanin in Appressorium Function. *Exp. Mycol.* 1989, **13**, 403–18
- Bechinger, C., Giebel, K.-F., Schnell, M., Leiderer, P., Deising, H.B., and Bastmeyer, M. Optical measurements of invasive forces exerted by appressoria of a plant pathogenic fungus. *Science* 1999, **285**, 1896–99
- Bell, A.A., and Wheeler, M.H. Biosynthesis and functions of fungal melanins. *Annu. Rev. Phytopath.* 1986, **24**, 411–51
- Tokousbalides, M.C., and Sisler, H.D. Effect of tricyclazole on growth and secondary metabolism in *Pyricularia oryzae*. *Pestic. Biochem. Physiol.* 1978, **8**, 26–32
- Woloshuk, C.P., Wolkow, P.M., and Sisler, H.D. The effect of three fungicides, specific for the control of rice blast, on the growth and melanin biosynthesis of *Pyricularia oryzae* Cav. *Pestic. Sci.* 1981, **12**, 86–90
- Ishida, M., and Nambu, K. Phthalide (Rabicide). *Noyaku Kagaku* 1975, **3**, 10–26
- Tsuji, G., Takeda, T., Furusawa, I., Horino, O., and Kubo, Y. Carpropamid, an anti-rice blast fungicide, inhibits scytalone dehydratase activity and appressorial penetration in *Colletotrichum lagenarium*. *Pestic. Biochem. Physiol.* 1997, **57**, 211–219
- Kurahashi, Y., Sakawa, S., Kinbara, T., Tanaka, K., and Kagabu, S. Biological activity of carpropamid (KTU 3616). A new fungicide for rice blast disease. *Nippon Noyaku Gakkaishi* 1997, **22**, 108–112
- Lundqvist, T., Rice, J., Hodge, C.N., Basarab, G.S., Pierce, J., and Lindqvist, Y. Crystal-structure of scytalone dehydratase—A disease determinant of the rice pathogen, *Magnaporthe grisea*. *Structure (London)* 1994, **2**, 937–944
- Chen, J.M., Xu, S.L., Wawrzak, Z., Basarab, G.S., and Jordan, D.B. Structure-based design of potent inhibitors of scytalone dehydratase: Displacement of a water molecule from the active site. *Biochemistry* 1998, **37**, 17735
- Basarab, G.S., Jordan, D.B., Gehret, T.C., Schwartz, R.S., and Wawrzak, Z. Design of scytalone dehydratase inhibitors as rice blast fungicides: derivatives of norephedrine. *Biorg. Med. Chem. Lett.* 1999, **9**, 1613
- Jordan, D.B., Lessen, T., Wawrzak, Z., Bisaha, J.J., Gehret, T.C., Hansen, S.L., Schwartz, R.S., and Basarab, G.S. Design of scytalone dehydratase inhibitors as rice blast fungicides: (N-phenoxypropyl)-carboxamides. *Biorg. Med. Chem. Lett.* 1999, **9**, 1607–1612
- Basarab, G.S., Steffens, J.J., Wawrzak, Z., Schwartz, R.S., Lundqvist, T., and Jordan, D.B. Catalytic mechanism of scytalone dehydratase: Site-directed mutagenesis, kinetic isotope effects, and alternate substrates. *Biochemistry* 1999, **38**, 6012–6024
- Wawrzak, Z., Sandolova, T., Steffens, J.J., Basarab, G.S., Lundqvist, T., Lindqvist, Y., and Jordan, D.B. High-resolution structures of scytalone dehydratase-inhibitor complexes crystallized at physiological pH. *Proteins Struct. Funct. Genet.* 1999, **35**, 425–39
- Manimaran, T., and Ramakrishnan, V.T. Synthesis of coumarins, thiocoumarins, and carbostyrils. *Ind. J. Chem.* 1979, **18B**, 324–330
- Baron, M.L., Martin, L.L., Rae, I.D., Simmonds, P.M., and Woolcock, M.L. Relaxation processes in aromatic methyl groups. II Methyl-methyl nuclear overhauser enhancements. *Aust. J. Chem.* 1990, **43**, 741–747
- Shnidhar, D.R., Jogibhukta, M., and Krishnan, V.S.H. A general and convenient synthesis of 2H-1,4-Benzoxazin-3(4H)-ones. *Org. Prep. Proc. Int.* 1982, **14**, 195–224
- Coutts, R.T., Hindmarsh, K.W., and Myers, G.E. Quinoline N-oxides and hydroxamic acids with antibacterial properties. *Can. J. Chem.*, 1970, **48**, 2393–2396
- Bizzozero, N., Garanti, L., and Zecchi, G. Synthesis of 2-Substituted 4H-[1,2,4]Triazolo[5,1-c]benzoxazines. *Synthesis* 1979, 909–910
- Garanti, L., Scandroglio, A., and Zecchi, G. Synthesis of fused ring 1,2,4-triazoles by intramolecular cycloaddition of nitrile imines to the nitrile function. *J. Heterocyclic Chem.* 1976, **13**, 1339–1341
- O'Sullivan, D.G., and Sadler, P.W. Vibrational frequency correlations in heterocyclic molecules. Part III. Carbonyl frequencies of certain compounds possessing fused six-membered rings. *J. Chem. Soc.* 1957, 2916–2920
- Gauthier, J., and Duceppe, J.S. Synthesis of novel imidazo[1,2-a][3,1]benzothiazines **4**, imidazo[1,2-a][1,2,4]benzotriazines **5**, and 4H-imidazo[2,3-c]pyrido[2,3-e][1,4]oxazines **6**. *J. Heterocyclic Chem.* 1984, **21**, 1081–1082
- Fusco, R., Garanti, L., and Zecchi, G. Intramolecular 1,3-dipolar cycloadditions of aryl azides bearing alkenyl, alkynyl, and nitrile groups. *J. Org. Chem.* 1975, **40**, 1906–1909
- Seki, T., Tasaka, S., and Hoshino, R. *Preparation and formulation of imidazo[2,1-β]benzothiazole derivatives as antiulcer agents*. 1990, EP347880
- Stjernloff, P., Elebring, T., Andersson, B., Svensson, A., Svensson, K., Ekman, A., Carlson, A., and Wikstrom, H. 5-, 6-, 7- and 8-amino-2-(N,N-di-n-propylamino)-1,2,3,4-tetrahydronaphthalenes: centrally acting DA and 5-HT<sub>1A</sub> agonists. *Eur. J. Med. Chem.*, 1993, **28**, 693–701
- Schenone, P., Mosti, L., and Menozzi, G. Reaction of 2-dimethylaminomethylene-1,3-diones with dinucleophiles. I. Synthesis of 1,5-disubstituted 4-acylpyrazoles. *J. Heterocyclic Chem.*, 1982, **19**, 1355–1361
- Avidon, V.V., and Shchukina, M.N. Synthesis of some substituted imidazo[5,1-b]benzothiazoles. *Khim. Geterotsikl. Soed. Akad. Nauk. Latv. SSR* 1965, **3**, 349–353
- Aryuzina, V.M., and Shchukina, M.N. The synthesis of substituted imidazo[5,1-b]benzimidazoles. III. 1,4-Dimethyl- and 4-benzylimidazo[5,1-b]benzimidazoles. *Khim. Geterotsikl. Soedin.* 1968, **4**, 509–11
- Mitschker, A., and Wedemeyer, K. The synthesis of substituted 1,2,3-benzotriaz-4(3H)-one N2-oxides and heteroannulated 1,2,3-Triazin-4(3H)-one N2-oxides. *Synthesis*, 1988, 517–520
- Lange, N.A., and Schiebley, F.E. Benzoylene Urea. *Org. Syn.* 1937, **XVII**, 16–17
- Elslager, E.F., Hess, C., Johnson, J., Ortwine, D., Chu, V., and Werbel, L. M. Synthesis and antimalarial effects of N2-Aryl-N4-[(dialkylamino)alkyl]- and N4-Aryl-N2-[(dialkylamino)alkyl]-2,4-quinazolinediamines. *J. Med. Chem.* 1981, **24**, 127–140
- Baker, B.R., Joseph, J.P., Schaub, R.E., McEvoy, F.J., and Williams, J.H. An antimalarial alkaloid from hydrangea. XIX. Thiophene isosteres. *J. Org. Chem.* 1952, **17**, 132–140
- Andersson, A., Jordan, D., Schneider, G., and Lindqvist, Y. Crystal structure of the ternary complex of 1,3,8-trihydroxynaphthalene reductase from *Magnaporthe*

- grisea* with NADPH and an active-site inhibitor. *Structure (London)* 1996, **4**, 1161–1170
- 34 Andersson, A.V., Basarab, G.S., Jordan, D.B., Liao, D.-I., Lindqvist, Y., Schneider, G. *Trihydroxynaphthalene reductase: methods for three dimensional structure determinations and rational inhibitor design*. 1999, PCT Int. Appl., 391 pp. WO 9919465 A1, 19990422, WO 98-US21550, 19981013
  - 35 Liao, D.-I., private communication
  - 36 Thompson, J.E., Basarab, G.S., Andersson, A., Lindqvist, Y., and Jordan, D.B. Trihydroxynaphthalene reductase from *Magnaporthe grisea*: Realization of an active center inhibitor and elucidation of the kinetic mechanism. *Biochemistry* 1997, **36**, 1852–1860
  - 37 Weiner, S.J., Kollman, P.A., Case, D.A., Chandra Singh, U., Ghio, C., Alagona, G., Profeta, S., and Weiner, P. A new force field for molecular mechanical simulation of nucleic acids and proteins. *J. Am. Chem. Soc.* 1984, **106**, 765–784
  - 38 Chandra Singh, U., Kollman, P.A. An approach to computing electrostatic charges for molecules. *J. Comp. Chem.* 1984, **5**, 129–145
  - 39 Clark, M., Cramer, R.D., and van Opdenbosch, N. Validation of the general purpose Tripos 5.2 force field. *J. Comput. Chem.* 1989, **10**, 982–1012
  - 40 Goodford, P.J. A computational procedure for determining energetically favourable binding sites on biologically important macromolecules. *J. Med. Chem.* 1985, **28**, 849–857
  - 41 Abraham, M.H., Duce, P.P., Prior, D.V., Barratt, D.G., Morris, J.J., and Taylor, P.J. Hydrogen bonding. Part 9. Solute proton donor and proton acceptor scales for use in drug design. *J. Chem. Soc. Perk. Trans. II* 1989, 1355–1375
  - 42 Taft, R.W., Gal, J.-F., Geribaldi, S., and Maria, P.C. Unique basicity properties of conjugated aminocyclohexenone derivatives. Effects of molecular structure on the disparate basicities towards H acids. *J. Am. Chem. Soc.* 1986, **108**, 861–863
  - 43 Kellogg, G.E., Semus S.F., and Abraham, D.J. *J. Comput. Aided Mol. Design.*, 1991, **5**, 545
  - 44 Andersson, A., Jordan, D., Schneider, G., and Lindqvist, Y. A flexible lid controls access to the active site in 1,3,8-trihydroxynaphthalene reductase. *FEBS Lett.* 1997, **400**, 173–176